Front. Mech. Eng. 2017, 12(4): 574–580
DOI 10.1007/s11465-017-0485-3

RESEARCH ARTICLE

Shota SANDO, Bo ZHANG, Tianhong CUI

Shrink-induced graphene sensor for alpha-fetoprotein detection with low-cost self-assembly and label-free assay

Abstract Combination of shrink induced nano-composites technique and layer-by-layer (LbL) self-assembled graphene challenges controlling surface morphology. Adjusting shrink temperature achieves tunability on graphene surface morphology on shape memory polymers, and it promises to be an alternative in fields of high-surface-area conductors and molecular detection. In this study, self-assembled graphene on a shrink polymer substrate exhibits nanowrinkles after heating. Induced nanowrinkles on graphene with different shrink temperature shows distinct surface roughness and wettability. As a result, it becomes more hydrophilic with higher shrink temperatures. The tunable wettability promises to be utilized in, for example, microfluidic devices. The graphene on shrink polymer also exhibits capability of being used in sensing applications for pH and alpha-fetoprotein (AFP) detection with advantages of label free and low cost, due to self-assembly technique, easy functionalization, and antigen-antibody reaction on graphene surface. The detection limit of AFP detection is down to 1 pg/mL, and therefore the sensor also has a significant potential for biosensing as it relies on low-cost self-assembly and label-free assay.

Keywords graphene, self-assembly, shrink polymer, AFP, label-free, biosensor

1 Introduction

Graphene has attracted great attention since its discovery due to the intriguing electrical and mechanical properties [1]. There has been a variety of applications of graphene reported in the last decade, and researchers continue to seek further applications, such as biosensing and electrochemiluminescence [2]. Graphene production method is one of the most important factors in practice as it is known as a one-atom-thickness carbon sheet. There are several techniques to produce graphene, though they still rely on sophisticated systems that are expensive and time-consuming [3]. Mechanical exfoliation method was initially proposed to obtain a single layer of graphene [4,5]. In this method, a piece of adhesive tape is used as an exfoliating material on which the peeled fragments from high quality graphite leave some layers of graphene. This method can provide the best quality of graphene. However, it requires technique and is difficult to control a number of layers of graphene, indicating difficulty with repeatability. As an alternative method to obtain graphene, chemical vapor deposition method has been developed [6,7]. In this method, copper foils are typically selected as substrates on which graphene is formed from decomposition of methane gas. Interestingly, it also enables to controlling graphene growth by adjusting heat-cool cycles [8]. There are other methods to make graphene reported in last decade, such as graphene epitaxy on silicon carbide [9], longitudinal unzipping of carbon nanotubes [10], but those methods have a lot of steps on the fabrication procedures and require expensive systems.

Layer-by-layer (LbL) self-assembly method presented in this work promises to be simple and widely applicable to graphene fabrication process. This method is a typical molecular self-assembly (MSA) by which target molecules assemble themselves without any help from outside interaction, and also known as one of bottom-up nanofabrication methods [11]. In this approach, graphene nanoplatelets can directly form several layers of graphene sheet on a desired substrate, and therefore it eliminates steps in which formed graphene is transferred onto a prepared substrate in conventional methods. It promises that graphene self-assembly can be used in further applications, such as micro-electro-mechanical systems (MEMS) [12]. By applying the method, we report experimental results in controlling surface morphology

Received December 23, 2016; accepted September 4, 2017

Shota SANDO, Bo ZHANG, Tianhong CUI (✉)
Department of Mechanical Engineering, University of Minnesota, Minneapolis, MN 55455, USA
E-mail: tcui@me.umn.edu

with both self-assembled graphene nanoplatelets and shrink-induced polymer structures [13]. Through our experiments, we demonstrated tunability of shrink induced self-assembled graphene on shape-memory polymers adjusted by shrink temperatures, and this promises to widen the range of graphene applications to high-surface-area conductors and molecular detections [14]. In addition, the technique was capable to change roughness, wettability, and the feature size of nanowrinkles. Compared with conventional methods for fabrication of graphene based nanostructures and devices, the combination of LbL self-assembly and shape memory polymers as the substrate demonstrates a relatively low-cost and simple process because of no requirements for sophisticated systems such as chemical vapor deposition and lithography.

This work also shows capability of sensors based on shrink-induced self-assembled graphene for an application to label-free molecule detections. In fact, there are tremendous amount of applications of biosensors based on electrochemistry in biosensing fields. pH sensors and glucose sensors are good example [15,16]. The major approach for bimolecular detection is utilizing a field effect transistor (FET) because it is very sensitive to changes in electrical charges on its surface caused by the adsorbed biomolecules. This indicates great potential for label-free biosensors. For this reason, while the methods based on fluorescence, such as enzyme-linked immunosorbent assay (ELISA), are still the most popular method to detect specific proteins in today's medicine in terms of detection of tumor biomarkers, label-free biosensors based on electrochemical immunoassay have attracted great attention due to their simple installation, low-cost, and easy operation [17,18]. The sensor in this paper demonstrates the detection of alpha-fetoproteins (AFP), one of the most important biomarkers associated with liver cancer and ovarian cancer. The high surface-to-volume ratio due to the nanowrinkles is expected to result in high antibody-capturing efficiency, higher sensitivity, and lower detection limit [19]. The results indicate shrink-induced graphene is practically applicable to high-performance biosensors in a wide range.

2 Materials and methods

2.1 LbL self-assembled graphene

LbL self-assembly method requires three types of charged suspensions in order to form graphene sheets from graphene nanoplatelets. The solutions used in this study were poly(diallyldiamine chloride) (PDDA, positively charged), poly(styrene sulfonate) (PSS, negatively charged), and pristine graphene platelets solution. The concentrations of PDDA and PSS were adjusted to 1.5 wt% and 0.3 wt%, respectively. PureSheets MONO (1-/2-layer graphene, 0.25 mg/mL) from NanoIntegris Technologies Inc., was used as graphene suspension solution (negatively charged).

Polystyrene (PS), known as a shrinkable polymer, was used as a substrate. The substrate was immersed in three solutions with following sequence: [PDDA (10 min) + PSS (10 min)]$_2$ + [PDDA (10 min) + graphene suspension (20 min)]$_5$. Herein, the PDDA/PSS layers were necessary for cleaning and initializing total charges on the substrate surface, so that layers of graphene sheets were uniformly formed on the PS substrate after the LbL cycle (Fig. 1). The PS substrate can shrink by heating over 100 ºC while the graphene sheets are not shrinkable. Hence, this mismatch of shrinkability after heating induces nanowrinkles on the graphene surface.

2.2 Sensors and functionalization for AFP detection

Electrodes were directly deposited by silver conductive paint (conductive epoxy purchased from Chemtronics, Inc.) on the PS substrate after heating (Fig. 2(a)). For AFP detection, poly-L-lysine (PLL) solution (0.1%w/v), Dulbecco's phosphate buffer solution (DPBS), bovine

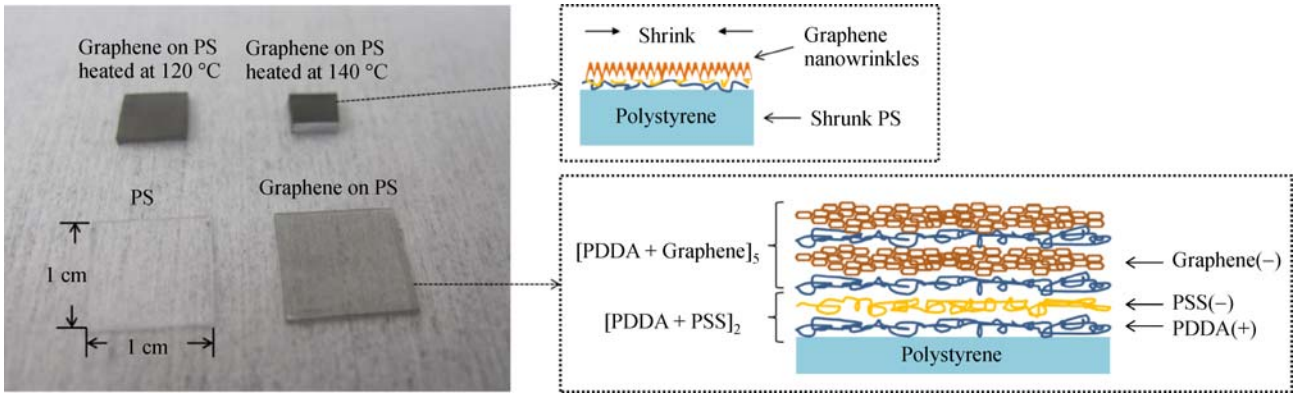

Fig. 1 Optical image of 1 cm × 1 cm polystyrene (PS) substrates with and without LbL self-assembled graphene and graphene on a PS substrate after heating at 120 ºC and 140 ºC, showing shrinkage and transparency change

serum albumin (BSA) solution (7.5%), and anti-AFP (rabbit, 0.05 mg/mL) were purchased from Sigma-Aldrich. Regarding functionalization, the graphene region, a sensing area, was immersed in PLL solution for 1 h at room temperature, and then washed three times by deionized (DI) water. Next, the sensor was immersed in anti-AFP solution (antibodies) which was diluted down to 1 μg/mL and stored in a refrigerator overnight. The sensing area was rinsed by DPBS to wash out excess of antibodies, and then BSA solution (2%) was applied onto it. The sensor was kept at room temperature for 2 h and washed by DPBS again. BSA is of importance for blocking nonspecific adsorption. If no blocking agent, undesired molecules can either be absorbed or sink on the sensing surface, and as a result, it causes signal fluctuation [20]. The sensor was immediately used after the cycle of antibody modification.

3 Results and discussion

3.1 Graphene surface properties

Since layers of graphene sheets on a PS substrate are very thin, the surface is transparent. When heated, the mismatch of interface between PS and graphene sheets causes nanowrinkles and increases the density of graphene. Figure 1 shows that graphene sheets on PS substrate obviously became opaque after heating at 120 ºC and 140 ºC, compared with before heating. We also took images of the graphene surface on the PS substrate before and after shrink using scanning electron microscope (SEM, JEOL 6500F). The surface of graphene sheets before heating was flat, which indicates no nanowrinkles and minimum density (Figs. 2(b) and 2(c)). The surface after heating, on the contrary, showed tremendous amount of nanowrinkles (Figs. 2(d)–2(g)). In addition, the results show that higher shrink temperature induce relatively larger and rougher nanowrinkles. To ensure the outcome, measurement of shrink rate of a PS substrate was carried out. The PS substrate with dimension of 1 cm × 2 cm were prepared for this experiment and heated in an oven for 10 min with different temperature. As shown in Fig. 3, the higher shrink temperature results in a higher shrink rate, and the PS substrate starts to shrink at 100 ºC. Herein, the following equation was used for the shrink rate calculation.

$$Shrink\ \ rate = \frac{s_0 - s_T}{s_0} \times 100\%, \tag{1}$$

where S_0 is the initial area of the PS substrates (1 cm × 2 cm = 2 cm^2) and S_T is the area after heating at T ºC. From the equation for shrink rate, the rate of surface area of graphene sheets, relative to the substrate, is quantitively calculated by the reciprocal of shrink rate. The actual area of the PS substrate gets relatively smaller with higher temperature, resulting in higher density of graphene. This relation also leads to higher roughness of graphene sheets on a PS substrate.

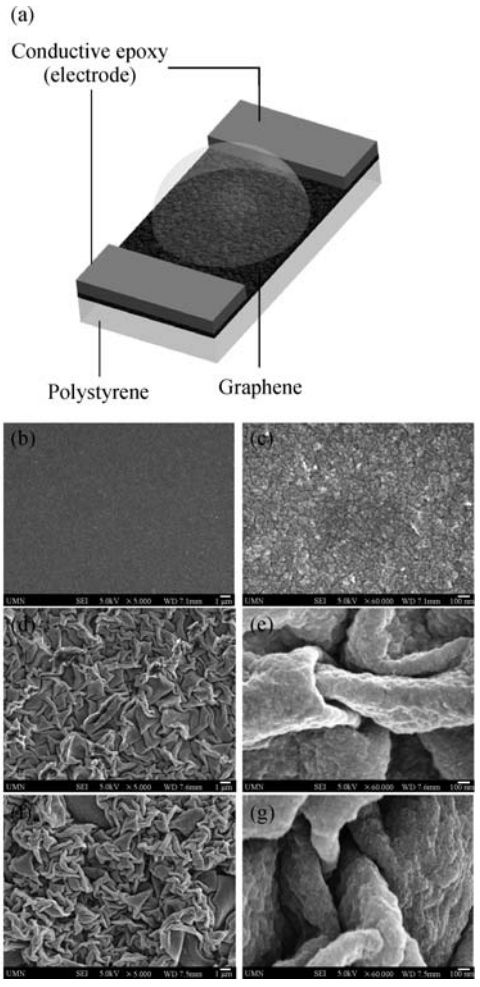

Fig. 2 (a) Schematic of LbL self-assembled graphene sensor; (b), (c) SEM image of graphene on a PS substrate before heating; (d), (e) SEM image of graphene on a PS substrate heated at 120 ºC; (f), (g) SEM image of graphene on a PS substrate heated at 140 ºC; magnification for (b) and (d), and (f) is × 5000; magnification for (c), (e), and (g) is × 60000

Wettability of graphene surface for different shrink temperatures was measured by contact angle meter (Fig. 4). As expected, the contact angle became smaller with increase of shrink temperature (increase of roughness), indicating that adjustment of shrink temperature enables to tuning graphene surface profile with respect to roughness and area. Here, Wenzel's model explains a relation between contact angle and surface roughness by the following equation:

$$\cos\theta^* = r\cos\theta, \tag{2}$$

where θ^* is the apparent (measured) contact angle, r is the ratio of actual and projected surface area (roughness ratio),

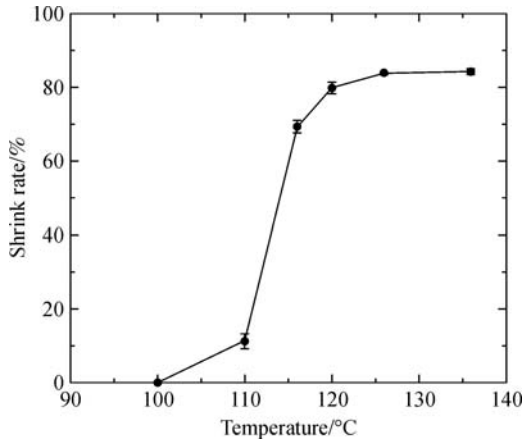

Fig. 3 Shrink rate of PS substrates with different temperature ($n = 5$)

and θ is the Young contact angle. From this equation, hydrophilic surface ($\theta^* < 90^o$) becomes more hydrophilic with roughness, and in contrast, hydrophobic surface ($\theta^* > 90^o$) becomes more hydrophobic with roughness. This is in good agreement with our results shown in Fig. 4. We believe that the graphene sheets on a shrink polymer substrate with tunable roughness of nanowrinkles and wettability have a considerable potential in microfluidics applications

3.2 pH sensing

Demonstrating a capability of use of graphene sheets on a PS substrate in a sensor application is of importance for showing its wide range of applications. We first tested pH response without any functionalization onto the graphene surface after heating. Phosphate buffer saline (PBS) were prepared for this experiment with three different pH values (5.31, 7.1, and 8). The buffer solutions were introduced onto the sensor, and the resistance shift was monitored by Agilent Data logger (34970A, Agilent, Inc.). As shown in Fig. 5, the resistance shifted up with decrease of pH although as-prepared sensors do not have selectivity to both hydroxonium ions (H_3O^+) and hydroxyl ions (OH^-). However, since both of ions working as acceptors and donors are able to lead the modulation of the graphene channel conductance due to its ambipolar characteristic, and the segregation of ions at the graphene/electrolyte interface was reported [21], the sensor can expectedly respond to pH change with constant change in resistance.

Self-assembled graphene sheets in this study showed p-type, which means the main carrier is a hole. This is consistent with the result from the pH measurement. Graphene shows variable Fermi level in the energy band and no potential barrier between graphene/solution interfaces, but it has limited density of state (DOS) [22]. Since hole is the main carrier, the Fermi level is located below the Dirac point where the effective mass is assumed to be zero with a high Fermi velocity (~108 cm/s). Lower pH results from higher concentration of H_3O^+ ions, and therefore, holes in the graphene repulsively recede from interface of the solution, consequently shifting the Fermi level up between the initial position and the Dirac point. As a result, resistance of graphene increases. The resistance shift can be also explained by Nernst equation in terms of potential shift at the graphene/electrolyte interface [23]. The general

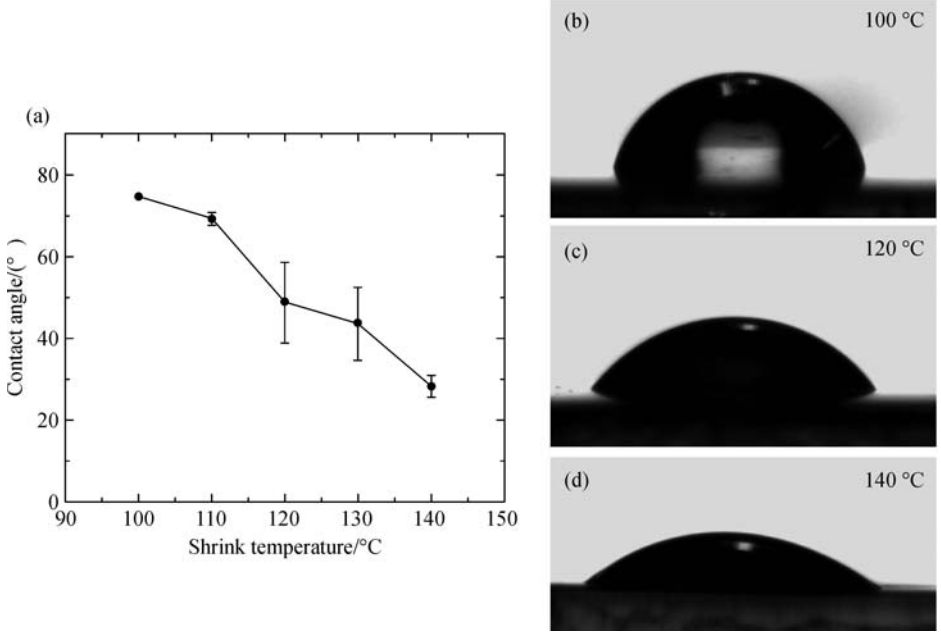

Fig. 4 (a) Wettability of graphene on PS substrates after heating ($n = 5$); (b)–(d) Optical images of droplet of DI water for contact angle measurement with different shrink temperature

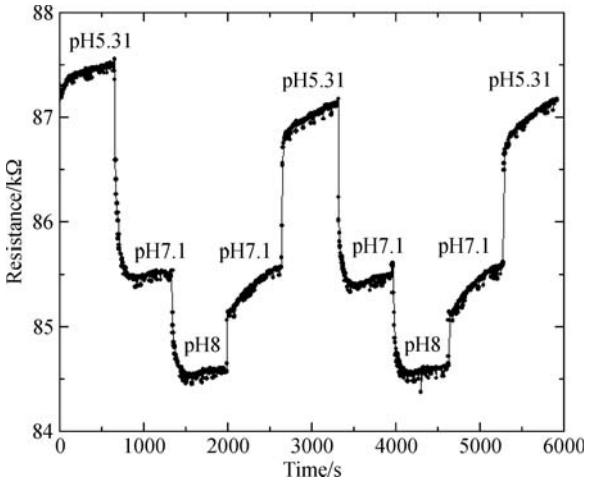

Fig. 5 Response of the sensor to pH (PBS, pH: 5.31, 7.1, 8.0) by resistance shift

expression for the sensitivity of the electrostatic potential to changes in the bulk pH is:

$$\frac{\delta\psi_0}{\delta \mathrm{pH}} = -2.3\frac{kT}{q}\alpha, \tag{3}$$

$$\alpha = \frac{1}{2.3kTC_{\mathrm{diff}}/(q^2\beta_{\mathrm{int}}) + 1}, \tag{4}$$

where ψ_0 is the change of the insulator-electrolyte potential, k is the Boltzmann constant, T is the absolute temperature, q is the elementary charge, α is a dimensionless sensitivity parameter, C_{diff} is the differential capacitance, and β_{int} is the intrinsic buffer capacity. α takes a value between 0 and 1 depending on C_{diff} and β_{int}. From the equation, the ideal surface potential shift is –59.2 mV/pH in case of α = 1. This potential shifts gate voltage in terms of graphene field effect transistor. The electrical characteristics of p-type graphene reveal on the left half from a vertex of its I_{d}-V_{g} curve, known as the Dirac point. The characteristics show that the resistance increases with increase of gate voltage (decrease of pH). Thus, the sensor is sensitive to changes of its environment.

3.3 Debye length for AFP sensing

In label-free AFP detection schemes based on graphene sensors, the surface of graphene used as a sensing material is functionalized with AFP antibodies as specific receptors that enable capturing target antigens. The graphene varies its resistance (conductance) with change of the surface potential caused by the accumulation of ions from the bound AFP antigens. However, unless the charge from the antibodies is enough closer to the surface, graphene cannot sense the potential change due to canceling out the total charge by counter ions. This is called Debye screening effect, and the distance from the surface that the effect of the counter ions becomes greater has an exponential behavior, $\exp(-x/\lambda_{\mathrm{D}})$. Here, λ_{D} is known as Debye length and defined by the following equation [24,25].

$$\lambda_{\mathrm{D}} = \frac{1}{\sqrt{8\pi l_{\mathrm{B}} N_{\mathrm{A}} I}}, \tag{5}$$

where l_{B} is the Bjerrum length (= 0.7 nm for water at room temperature), N_{A} is the Avogadro constant, and I is the ionic strength defined by the following equation.

$$I = \frac{1}{2}\sum\nolimits_{i=1}^{n} C_i Z_i^2, \tag{6}$$

where C_i is the molar concentration of ion i and Z_i is the charge number of ion i. The ionic strength of DPBS used in this study is 154.4 mmol/L which corresponds to 0.78 nm of the Debye length. For AFP antigens captured by the antibodies, detecting its charge is affected by Debye screening effect.

Diluting test sample is one of effective approaches in order to deal with the Debye length problem [26]. Figure 6 shows the calculated result of the Debye length and ionic strength with different dilution rate of DPBS. To detect the target antigens which require more than 20 nm of the Debye length, 0.001 of dilution rate (1000 times of dilution) is desired.

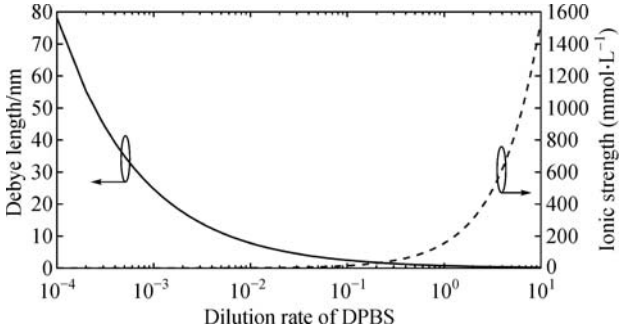

Fig. 6 Dilution rate of DPBS vs. Debye length (solid line) and Dilution rate of DPBS vs. Ionic strength (dashed line)

3.4 AFP detection

For the biosensor application, AFP detection by the sensor was carried out. The sensor was characterized by applying DPBS containing different concentration of AFP antigens after immobilization of AFP antibodies onto the sensing surface according to aforementioned method.

Ideally, the testing solution should be diluted for adjustment of the Debye length. This ensures that the Debye length is well above the length of antigen-antibody complexes, and is of importance for sensors in order to obtain unambiguous response caused by the antigen-antibody reaction. However, taking a step of dilution is not practical in terms of actual diagnosis due to either an extra requirement to superior detection limit or a risk of losing

target molecules in the sample. To overcome the problems, we used a technique which takes a procedure of changing ionic strength every after antigen-antibody reaction while monitoring [27,28].

We prepared two testing solutions, DPBS containing AFP antigens and diluted DPBS. The ionic strength of as-prepared DPBS was 154.4 mM which corresponds to 0.78 nm of the Debye length. On the other hand, ionic strength of diluted DPBS was adjusted down to 0.15 mmol/L (1000 times dilution), which is equal to 25 nm of the Debye length, and used as a reference buffer solution. The diluted DPBS was firstly introduced onto the sensing surface, and after stabilization of the output resistance, we exchanged the solution to DPBS with AFP antigens. After 30 min, enough time to reach equilibrium of the antigen-antibody reaction, we exchanged the solution back to the diluted DPBS. This procedure enabled adjusting the Debye length longer enough to detect captured AFP antigens while monitoring. We repeated this cycle several times for different concentration of AFP antigens.

Figure 7 shows good linearity of the normalized resistance shift in logarithmic function scale, corresponding to different concentration of AFP antigens. The normalized resistance was used in order to obtain clear readout and to cancel out individual difference of sensors. The resistance for the diluted DPBS before introducing any AFP antigens was used as an initial resistance, R_0, and other resistance values for the diluted DPBS were used as R. ΔR is the difference between R and R_0, and therefore, the y-axis in Fig. 7 ($\Delta R/R_0$) corresponds to percentage of the resistance shift before and after antigen-antibody reaction for the reference buffer solution.

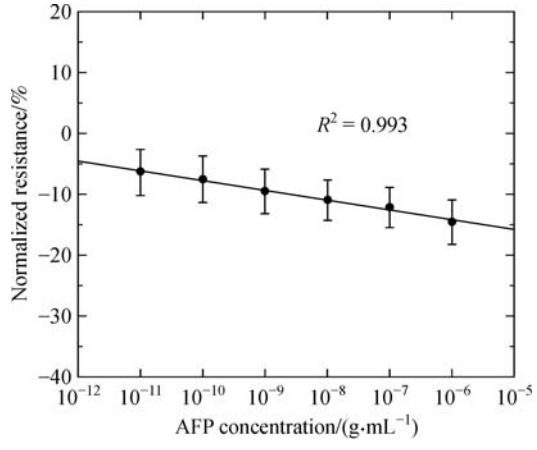

Fig. 7 AFP detection result in which Normalized resistance is represented as $\Delta R/R_0$ ($n = 4$)

AFP antigen is negatively charged in DPBS (pH ~7.3) because its isoelectric point (pI) is ~4.7. Therefore, the trend of resistance shift, decrease of resistance with increasing concentration of AFP antigens, was reasonable, and can be explained by the same discussion as the resistance shift in the pH sensing section (3.2). The sensor demonstrated lower detection limit down to 1 pg/mL. We estimate that changing graphene surface morphology with nanowrinkles played an important role of giving antigens and antibodies more chances to meet together due to rougher surface with larger area. This result promises the sensor has capability in use as a label-free AFP sensor.

We also demonstrated detecting AFP antigens for two solutions which have different Debye length. Figure 8 shows the resistance shift of graphene with different concentration of induced AFP antigen for the diluted DPBS and as-prepared DPBS. As expected, graphene showed obvious resistance shift with the diluted DPBS due to longer Debye length which enables graphene to sense the charge from captured antigens. On the other hand, it could not clearly perform sensing the antigens with as-prepared DPBS due to shorter Debye length. This result gives us good agreement with the Debye screening effect.

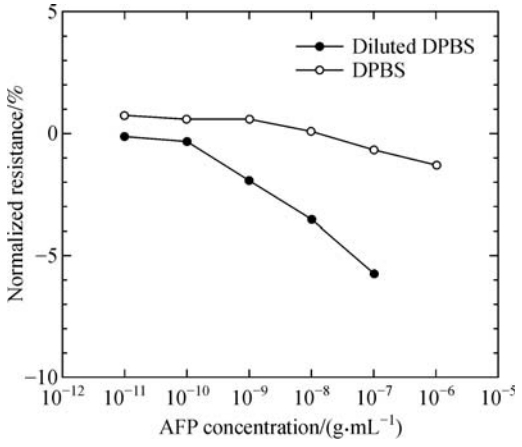

Fig. 8 Comparison of normalized resistance for the response to different concentration of AFP antigens between diluted DPBS and as-prepared DPBS

4 Conclusions

Shrink-induced LbL self-assembled graphene exhibited tunable surface properties and capability of being used as a biosensor. Utilization of shape memory polymers enables facile tuning of graphene surface by adjusting shrink temperature, resulting in changing surface roughness and wettability. Sensitivity of graphene sheets with nanowrinkles to exposure of the surface was also investigated, and the response was good enough to detect captured antigens based on the antigen-antibody reaction. Considering the Debye screening effect is also of importance for practical applications, and we can overcome the issue by adjusting the Debye length with the reference solution. In addition, we successfully achieved development of a relatively low-cost and label-free sensor due to its simple fabrication process and ease of surface modification.

The sensor holds enormous potential for being used in

microfluidics and biosensors. We will continue to investigate further applications of tunable shrink-induced LbL self-assembled graphene sheets.

Acknowledgements The authors acknowledge the assistance of fabrication and characterization from Minnesota Nano Center and the Characterization Facility at the University of Minnesota.

References

1. Schwierz F. Graphene transistors. Nature Nanotechnology, 2010, 5 (7): 487–496
2. Chen D, Tang L, Li J. Graphene-based materials in electrochemistry. Chemical Society Reviews, 2010, 39(8): 3157–3180
3. Yang W, Ratinac K R, Ringer S P, et al. Carbon nanomaterials in biosensors: Should you use nanotubes or graphene? Angewandte Chemie International Edition, 2010, 49(12): 2114–2138
4. Novoselov K S, Geim A K, Morozov S V, et al. Electric field effect in atomically thin carbon films. Science, 2004, 306(5696): 666–669
5. Blake P, Hill E W, Castro Neto A H, et al. Making graphene visible. Applied Physics Letters, 2007, 91(6): 063124
6. Li X, Cai W, An J, et al. Large-area synthesis of high-quality and uniform graphene films on copper foils. Science, 2009, 324(5932): 1312–1314
7. Mattevi C, Kim H, Chhowalla M. A review of chemical vapour deposition of graphene on copper. Journal of Materials Chemistry, 2011, 21(10): 3324–3334
8. Yu Q, Jauregui L A, Wu W, et al. Control and characterization of individual grains and grain boundaries in graphene grown by chemical vapour deposition. Nature Materials, 2011, 10(6): 443–449
9. Sutter P. Epitaxial graphene: How silicon leaves the scene. Nature Materials, 2009, 8(3): 171–172
10. Kosynkin D V, Higginbotham A L, Sinitskii A, et al. Longitudinal unzipping of carbon nanotubes to form graphene nanoribbons. Nature, 2009, 458(7240): 872–876
11. Biswas A, Bayer I S, Biris A S, et al. Advances in top–down and bottom–up surface nanofabrication: Techniques, applications & future prospects. Advances in Colloid and Interface Science, 2012, 170(1–2): 2–27
12. Wei W, Song Y, Wang L, et al. An implantable microelectrode array for simultaneous L-glutamate and electrophysiological recordings *in vivo*. Microsystems & Nanoengineering, 2015, 1: 15002
13. Sando S, Zhang B, Cui T A. Low-cost and label-free alpha-fetoprotein sensor based on self-assembled graphene on shrink polymer. In: Proceedings of 2015 28th IEEE International Conference on Micro Electro Mechanical Systems (MEMS). Estoril: IEEE, 2015, 324–327
14. Fu C, Grimes A, Long M, et al. Tunable nanowrinkles on shape memory polymer sheets. Advanced Materials, 2009, 21(44): 4472–4476
15. Sohn I Y, Kim D J, Jung J H, et al. pH sensing characteristics and biosensing application of solution-gated reduced graphene oxide field-effect transistors. Biosensors & Bioelectronics, 2013, 45: 70–76
16. Anan H, Kamahori M, Ishige Y, et al. Redox-potential sensor array based on extended-gate field-effect transistors with ω-ferrocenylalkanethiol-modified gold electrodes. Sensors and Actuators B, Chemical, 2013, 187: 254–261
17. Patolsky F, Zheng G, Lieber C M. Fabrication of silicon nanowire devices for ultrasensitive, label-free, real-time detection of biological and chemical species. Nature Protocols, 2006, 1(4): 1711–1724
18. Chen X, Jia X, Han J, et al. Electrochemical immunosensor for simultaneous detection of multiplex cancer biomarkers based on graphene nanocomposites. Biosensors & Bioelectronics, 2013, 50: 356–361
19. Li X, Zhao C, Liu X. A paper-based microfluidic biosensor integrating zinc oxide nanowires for electrochemical glucose detection. Microsystems & Nanoengineering, 2015, 1: 15014
20. Hideshima S, Sato R, Inoue S, et al. Detection of tumor marker in blood serum using antibody-modified field effect transistor with optimized BSA blocking. Sensors and Actuators B, Chemical, 2012, 161(1): 146–150
21. Cole D J, Ang P K, Loh K P. Ion adsorption at the graphene/electrolyte interface. Journal of Physical Chemistry Letters, 2011, 2 (14): 1799–1803
22. Nagashio K, Toriumi A. Density-of-states limited contact resistance in graphene field-effect transistors. Japanese Journal of Applied Physics, 2011, 50(7R): 070108
23. van Hal R E G, Eijkel J C T, Bergveld P. A novel description of ISFET sensitivity with the buffer capacity and double-layer capacitance as key parameters. Sensors and Actuators B, Chemical, 1995, 24(1–3): 201–205
24. Israelachvili J N. Intermolecular and Surface Forces. 3rd ed. Amsterdam: Elsevier, 2011
25. Vacic A, Criscione J M, Rajan N K, et al. Determination of molecular configuration by Debye length modulation. Journal of the American Chemical Society, 2011, 133(35): 13886–13889
26. Park C W, Ah C S, Ahn C G, et al. Analysis of configuration of surface-immobilized proteins by Si nanochannel field effect transistor biosensor. Procedia Chemistry, 2009, 1(1): 674–677
27. Kim A, Ah C S, Park C W, et al. Direct label-free electrical immunodetection in human serum using a flow-through-apparatus approach with integrated field-effect transistors. Biosensors & Bioelectronics, 2010, 25(7): 1767–1773
28. Stern E, Wagner R, Sigworth F J, et al. Importance of the Debye screening length on nanowire field effect transistor sensors. Nano Letters, 2007, 7(11): 3405–3409